Neutron diffraction study of UO_2: Antiferromagnetic state*

J. Faber, Jr. and G. H. Lander
Materials Science Division, Argonne National Laboratory, Argonne, Illinois 60439
(Received 5 April 1976)

The elastic neutron magnetic scattering cross section from the U^{4+} ions in antiferromagnetic UO_2 has been measured at 4.2 K. The measurements included all reciprocal-lattice points for which $(\sin\theta)/\lambda = \kappa/4\pi \leq 0.83$ Å^{-1}. The values of $\mu f(\vec{\kappa})$, obtained from the measurements, fall on a smooth curve at small κ, but show considerable anisotropy for $(\sin\theta)/\lambda > 0.5$ Å^{-1}. The ordered magnetic moment is $(1.74 \pm 0.02)\mu_B$ per uranium atom at 4.2 K. Theoretical calculations of the magnetic cross section from a number of possible states (including the effects of intermediate coupling and J mixing) are unable to reproduce the experimental data at large κ. Subtracting the calculated magnetic cross section from the observed scattering cross section, we have determined that additional scattering is present only for reflections with h, k even and l odd. The additional intensity is a result of a small (0.014 Å) shift of the oxygen atoms from their equilibrium position. These shifts are examined within the framework of Allen's microscopic theory for UO_2. An analysis in terms of the homogeneous deformations proposed by Allen cannot explain the neutron results. However, when Allen's concepts are extended to include inhomogeneous deformations, corresponding to a zone-boundary $q = (2\pi/a)$ (1,0,0) phonon, excellent agreement is obtained between theory and experiment. The oxygen displacement is 0.014 Å from the fluorite lattice positions and, in addition, the inhomogeneous deformation $T_{2g} - T_{1g}$ does not require a corresponding change in the unit-cell dimensions. The dominance of this deformation mode in the spin-lattice interactions suggests the presence of a noncollinear magnetic structure in UO_2.

I. INTRODUCTION

The low-temperature antiferromagnetic properties of UO_2 were first examined by neutron diffraction about ten years ago.[1,2] Frazer *et al.*[1] considered in detail the first-order para- to antiferromagnetic transition in UO_2 at 30.8 K and presented a limited set of reflections to illustrate the variation of the effective form factor with scattering angle. Uranium dioxide has the face-centered-cubic (fcc) fluorite structure for the chemical unit cell. The magnetic structure, which is shown in Fig. 1, is type I, consisting of ferromagnetic (001) planes stacked in an alternating + – sequence. In a multidomain sample, the precise spin direction cannot be determined, but it does lie in the (001) plane, i.e., perpendicular to the propagation direction of the magnetic structure. No attempt was made by either Frazer *et al.*[1] or Willis and Taylor[2] to compare the observed magnetic form factor with theory. Since that time, the advent of the tensor-operator method[3,4] has made the calculation of magnetic scattering from systems such as UO_2 relatively easy.

The aim of the present experiment was to remeasure the magnetic scattering accurately and compare the results with theory. Such a comparison provides information on the spatial distribution of the two unpaired 5*f* electrons around each uranium ion and on possible covalent bonding effects. In addition, similar measurements on lanthanide systems[5] have shown that the symmetry of the crystal-field ground state gives rise to anisotropies in the magnetic form factor. In view of the anisotropy in the early UO_2 results,[1] a reasonable goal was the unique determination of the crystal-field ground state. This problem is complicated in the actinides by the presence of strong crystalline-field interactions that lead to intermediate coupling and J mixing.[6] The influence of these effects on the neutron cross sections have not been previously investigated. However, in the present experiment, considerably more anisotropy was observed at high scattering angles than expected on the basis of single-ion calculations.[7] Initial attempts to understand these effects were unsuccessful, despite the introduction of intermediate coupling and mixed-J wave functions. To obtain independent information on the magnetization density in UO_2, an experiment was conducted in the paramagnetic phase at 64 K. The results of this experiment, and an accompanying paper on the derivation of relativistic Dirac-Fock wave functions, have been published.[8,9] The magnetic form factor in the paramagnetic state is in excellent agreement with theory, suggesting that the scattering observed in the ordered state may not be representative of the magnetization density.

A detailed analysis of the neutron scattering cross section led us to consider the contamination of one particular subset of so-called magnetic Bragg reflections by nuclear scattering. This nuclear scattering arises as a result of displacements of the oxygen atoms from their ideal fluorite lattice sites. A brief account of how this internal rearrangement is related to the spin-lattice inter-

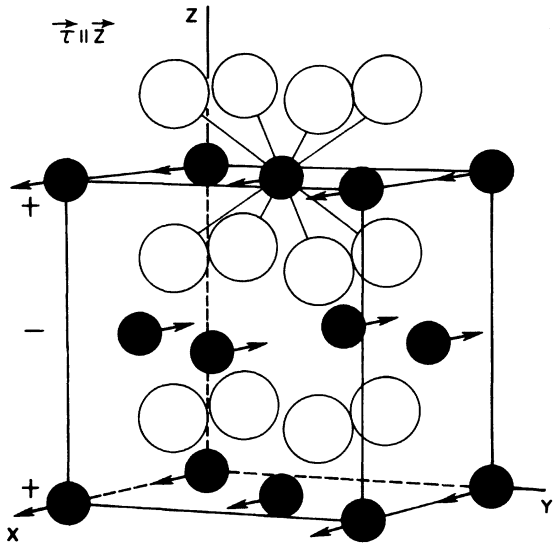

FIG. 1. Magnetic structure of UO_2. The propagation direction of the magnetic structure $\vec{\tau} \| \vec{z}$ and the uranium moments lie in the (001) plane. For convenience $\vec{\mu} \| \vec{x}$.

action in UO_2 has been presented.[10] The experiments are described in Sec. II. In Sec. III, details are given of the calculation of the magnetic cross section and the anisotropy that could be introduced as a result of the higher J-state configurations. In Sec. IV, the analysis starts with the subtraction of the "best" magnetic cross section from the observed data, and shows that the remaining neutron intensity is caused by an internal distortion of the oxygen sublattice. The implications of this internal distortion on the spin-lattice interaction and the well-accepted magnetic structure of UO_2 are also discussed.

II. EXPERIMENT

A UO_2 single crystal ($1.6 \times 2.4 \times 5.1$ mm) was cut from an arc-melt grown boule obtained from Savanah River some years ago. The long dimension of the crystal is parallel to a [110] axis. The stoichiometry was established[11] by heating the crystal in a 10^{-6} to 5×10^{-7} Torr vacuum at 2220 K; the lattice constant at 296 K, $a = 5.4702 \pm 0.0002$ Å, agrees well with values found in the literature.[12] Neutron-diffraction experiments were performed at the CP-5 Research Reactor using an instrument capable of collecting three-dimensional scattering data at low temperature.[13] The neutron wavelength $\lambda = 0.992$ Å was obtained with a Ge monochromator [the (311) reflection showed <0.01% contamination from $\frac{1}{2}\lambda$ and $\frac{1}{3}\lambda$]. To minimize systematic multiple scattering, the crystal was misoriented by 4° from the zone orientation.

A. Nuclear cross section

Specimen characterization as well as parameters needed in processing the magnetic intensities were obtained at 300, 80, and 4.2 K by measuring the nuclear Bragg scattering. To place the coherent elastic nuclear scattering in barns (b) on an absolute scale, we define the quantity

$$\left(\frac{d\sigma}{d\Omega}\right)_N = d\sigma_N = |N|^2 \quad \text{b/mole}, \tag{1}$$

where N is the nuclear structure factor per molecular unit. The nuclear structure factors for the ideal fluorite lattice can be expressed as

$$N_{hkl} = b_U e^{-W_U} \quad \text{if } h+k+l = 4n \pm 1 \tag{2a}$$

or

$$= b_U e^{-W_U} + 2b_0 e^{-W_0} \quad \text{if } h+k+l = 4n \tag{2b}$$

and

$$= b_U e^{-W_U} - 2b_0 e^{-W_0} \quad \text{for } h+k+l = 4n+2. \tag{2c}$$

The coherent scattering lengths of uranium and oxygen are $b_U = 0.853 \times 10^{-12}$ cm and $b_0 = 0.580 \times 10^{-12}$ cm, and e^{-W} are the Debye-Waller factors. The polarized-neutron experiments[9] on the same crystal of UO_2 confirm that the sample is close to stoichiometry and that the scattering lengths are correct. For a Bragg angle of θ, $d\sigma_N$ is related to

TABLE I. Results of refinements of the nuclear structure factors for UO_2 at 300, 80, and 4.2 K.

Parameter	$T = 300$ K $\lambda = 1.05$ Å	$T = 80$ K $\lambda = 0.992$ Å	$T = 4.2$ K $\lambda = 0.992$ Å
Scale constant	49.0(4)	50.4(2)	50.3(2)
Extinction parameter g	936(73)	1110(46)	1155(43)
B_U (Å^2)	0.25(2)	0.10(1)	0.07(1)
B_O (Å^2)	0.41(2)	0.24(1)	0.22(1)
χ^2	1.2	1.4	1.2
Residual (weighted) %	1.2	0.9	0.6
Number of observations	1250	594	540
Number of independent hkl's	24	32	32

the integrated intensity by

$$I_N = C|N|^2 Ay/\sin 2\theta, \quad (3)$$

where C is the overall scale factor, A is the absorption coefficient, and y is the extinction correction. Following Zachariasen,[14]

$$y = (1 + 2gQ\bar{t})^{-1/2}, \quad (4)$$

where $Q = \lambda^3 V^{-2}|N|^2/\sin 2\theta$, V is the volume of the unit cell, λ is the neutron wavelength, $\bar{t}$ is the effective path length, and g is the extinction parameter. We find the Zachariasen formula adequate to describe the extinction effects, which result in ~5% corrections for the $4n+2$ reflections, and the high value of g suggests type II extinction.[14] The neutron wavelength dependence of the extinction parameter is also consistent with type II behavior. The results of refining the nuclear structure factors, taken at various temperatures and neutron wavelengths, with a least-squares program are given in Table I. The crystallographic residuals of ~0.01 ($\chi^2 \sim 1.2$) confirm that the observed and calculated intensities are in excellent agreement for all temperatures investigated. In Fig. 2, the cross section, uncorrected for extinction, is plotted as a function of $h^2+k^2+l^2$. The solid lines are the theoretical values for the three types of structure factors in UO_2 [see Eq. (2)].

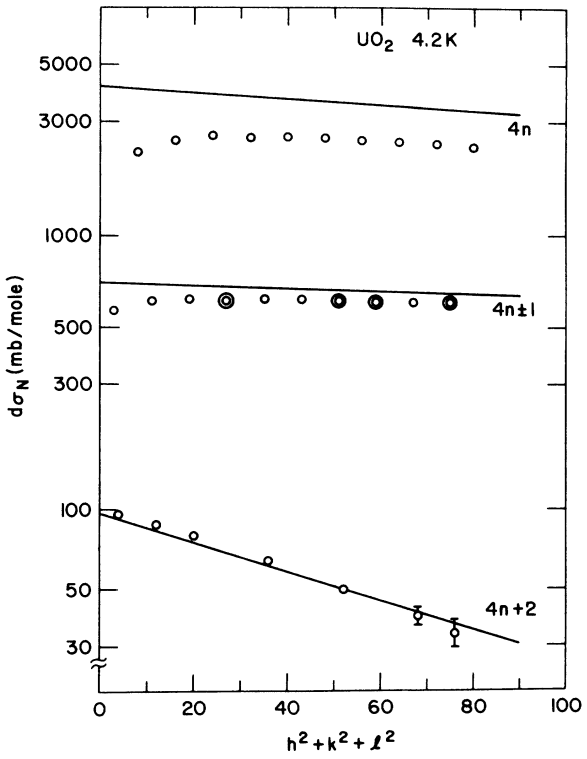

FIG. 2. Nuclear cross section as a function of the reflection indices. The experimental points have not been corrected for extinction. The straight lines correspond to the results of the least-squares analysis and include extinction. The double circles on the $4n \pm 1$ line signify pairs of reflections.

Neutron experiments on UO_2 at high temperature have indicated the presence of anharmonic effects,[15] which initially reduce the consistency of the $4n \pm 1$ reflections. If anharmonic effects were important, we would expect the $4n \pm 1$ pairs of reflections (double circles in Fig. 2) to have different intensities. The absence of any measurable differences in Fig. 2 shows that the effects of anharmonicity are too small to be observed at low temperature.

The most serious source of experimental uncertainty arises from the difficulty of eliminating or assessing the effects of multiple scattering. The high degree of internal consistency in sets of both nuclear and magnetic equivalent reflections and the low residuals given in Table I show that the effects of multiple scattering are at least small. A similar conclusion was reached after performing a number of azimuthal scans.[7] However, in the present experiment, we have measured magnetic intensities of <1 mb/mole (strong nuclear intensities are on the order of 3000 mb/mole), which suggests that even a small amount of multiple scattering could be the source of serious contamination. Indeed, analyses of the magnetic data (Sec. III) suggest that a small amount of additional intensity (~0.3 mb/mole) occurs at magnetic reciprocal lattice points, probably due to multiple scattering. It should be noted that the symmetry of the antiferromagnetic structure in UO_2 is such that interference between nuclear reflections cannot result in intensity at magnetic reciprocal lattice points. The unwanted multiple scattering will arise from nuclear-magnetic interference; hence, the absence of these small effects at temperatures above T_N does not constitute a complete check for multiple scattering.

B. Magnetic cross section

The magnetic structure of UO_2 is shown in Fig. 1. We have indexed the magnetic and nuclear reflections on the basis of the chemical unit cell. Magnetic reflections have indices such that $h+k$ = even and $h+l$ = odd. Since the chemical unit cell is face centered and gives rise to reflections with h,k,l all even or all odd, the magnetic and nuclear reflections are completely separated in reciprocal space. With this magnetic structure, reflections such as (011) and (101) should not be present. As illustrated in Fig. 1, the propagation direction of the magnetic structure $\vec{\tau}$ is parallel to one of the cube axes, in this case $\vec{c}$. However, $\vec{a}$- and $\vec{b}$-type

TABLE II. Experimental and theoretical results for UO_2. The observed cross section is $d\sigma_{obs}$, the calculated values for two models (Sec. III) is $d\sigma_M$. The cross section from the oxygen displacement (Sec. IV) is $d\sigma_D$.

hkl	$(\sin\theta)/\lambda$ (Å^{-1})	$\langle q^2\rangle$	$d\sigma_{obs}$ (mb/mole)	$^3H_4$ $d\sigma_M$ (mb/mole)	$4J$ $d\sigma_M$ (mb/mole)	$^3H_4$ $d\sigma_{obs}-d\sigma_M$ (mb/mole)	$d\sigma_D$ (mb/mole)
001	0.092	1.000	65.1(1.6)	66.69	64.95	−1.6(1.6)	0.00
110	0.130	0.500	31.3(6)	30.86	30.39	+0.4(6)	0.00
201	0.206	0.600	27.4(5)	27.73	27.73	−0.3(5)	0.23
112	0.225	0.833	34.0(6)	34.85	35.08	−0.8(6)	0.00
221	0.275	0.556	18.2(6)	18.26	18.92	−0.1(6)	0.46
003	0.275	1.000	32.5(5)	31.69	31.30	+0.8(5)	0.00
310	0.290	0.500	14.6(4)	14.74	14.72	−0.1(4)	0.00
203	0.331	0.846	18.9(5)	18.55	18.93	+0.4(5)	0.23
312	0.343	0.643	13.0(5)	13.34	14.21	−0.3(5)	0.00
401	0.378	0.529	9.8(4)	8.62	8.77	+1.2(4)	0.91
223	0.378	0.765	11.3(5)	11.54	12.52	−0.2(5)	0.45
330	0.389	0.500	8.4(5)	7.44	7.47	+1.0(5)	0.00
114	0.389	0.944	14.2(7)	13.41	13.37	+0.8(7)	0.00
421	0.420	0.524	7.3(4)	6.10	6.38	+1.2(4)	1.14
332	0.430	0.591	5.6(4)	6.02	6.91	−0.4(4)	0.00
403	0.458	0.680	6.6(4)	5.67	6.19	+0.9(4)	0.90
005	0.458	1.000	10.9(6)	8.54	8.38	+2.4(6)	0.00
510	0.467	0.500	4.4(5)	3.96	3.92	+0.4(5)	0.00
314	0.467	0.808	5.8(4)	5.56	5.89	+0.2(4)	0.00
423	0.494	0.655	5.0(5)	3.68	4.41	+1.3(5)	1.12
205	0.494	0.931	5.9(4)	5.31	5.22	+0.6(4)	0.22
512	0.502	0.566	3.8(6)	3.48	3.93	+0.3(6)	0.00
441	0.526	0.515	3.8(4)	2.07	2.05	+1.7(4)	1.79
225	0.526	0.879	3.9(4)	3.28	3.37	+0.6(4)	0.44
530	0.534	0.500	2.0(3)	1.98	1.88	0.0(3)	0.00
334	0.534	0.735	2.4(3)	2.31	2.88	+0.1(3)	0.00
601	0.558	0.514	4.4(3)	1.99	2.11	+2.4(3)	2.01
532	0.565	0.553	1.8(4)	1.60	1.95	+0.2(4)	0.00
116	0.565	0.974	3.6(4)	3.09	3.04	+0.5(4)	0.00
405	0.587	0.805	2.7(3)	1.66	1.70	+1.0(3)	0.88
443	0.587	0.610	3.0(7)	1.13	1.57	+1.9(7)	1.78
621	0.587	0.512	4.0(4)	1.43	1.58	+2.6(4)	2.22
514	0.594	0.690	1.8(5)	1.51	1.76	+0.3(5)	0.00
425	0.615	0.778	2.1(5)	0.98	1.16	+1.1(5)	1.10
603	0.615	0.600	3.8(4)	1.43	1.74	+2.4(4)	1.99
316	0.622	0.891	1.8(7)	1.25	1.22	+0.6(7)	0.00
007	0.641	1.000	3.6(9)	1.81	1.90	+1.8(9)	0.00
623	0.641	0.592	3.4(5)	0.95	1.31	+2.4(5)	2.20
534	0.648	0.660	0.8(3)	0.58	0.89	+0.2(3)	0.00
550	0.648	0.500	1.2(4)	0.44	0.26	+0.8(4)	0.00
207	0.667	0.962	2.0(4)	1.11	1.10	+0.9(4)	0.21
641	0.667	0.509	3.3(3)	0.46	0.46	+2.8(3)	2.85
712	0.673	0.537	1.1(5)	0.84	1.10	+0.3(5)	0.00
336	0.673	0.833	1.2(3)	0.44	0.51	+0.8(3)	0.00
227	0.692	0.930	1.3(3)	0.65	0.62	+0.6(3)	0.43
445	0.692	0.719	2.1(4)	0.23	0.39	+1.9(4)	1.74
730	0.698	0.500	0.8(4)	0.46	0.54	+0.3(4)	0.00
605	0.716	0.705	2.4(5)	0.43	0.48	+2.0(5)	1.95
643	0.716	0.574	3.1(4)	0.26	0.47	+2.8(4)	2.82
516	0.721	0.790	0.6(3)	0.32	0.36	+0.3(3)	0.00
732	0.721	0.532	0.6(2)	0.42	0.66	+0.2(2)	0.00
407	0.738	0.877	1.4(6)	0.33	0.35	+1.1(6)	0.86
625	0.738	0.692	2.8(7)	0.25	0.35	+2.6(7)	2.15
801	0.738	0.508	4.1(4)	0.45	0.57	+3.6(4)	3.46
554	0.744	0.621	0.8(4)	0.10	0.22	+0.7(4)	0.00

TABLE II *(Continued)*

hkl	$(\sin\theta)/\lambda$ (Å^{-1})	$\langle q^2\rangle$	$d\sigma_{obs}$ (mb/mole)	$^3H_4$ $d\sigma_M$ (mb/mole)	$4J$ $d\sigma_M$ (mb/mole)	$^3H_4$ $d\sigma_{obs}-d\sigma_M$ (mb/mole)	$d\sigma_D$ (mb/mole)
118	0.744	0.985	1.0(4)	0.66	0.73	+0.3(4)	0.00
427	0.761	0.855	1.4(5)	0.17	0.21	+1.2(5)	1.07
821	0.761	0.507	3.9(5)	0.36	0.51	+3.5(5)	3.66
536	0.766	0.757	0.4(3)	0.08	0.15	+0.3(3)	0.00
661	0.783	0.507	3.8(4)	0.05	0.03	+3.8(4)	3.86
803	0.783	0.562	3.8(5)	0.47	0.64	+3.3(5)	3.42
318	0.788	0.932	0.8(9)	0.26	0.26	+0.5(9)	0.00
734	0.788	0.608	0.5(2)	0.19	0.37	+0.3(2)	0.00
750	0.788	0.500	0.5(4)	0.09	0.10	+0.4(4)	0.01
645	0.804	0.662	2.8(5)	0.04	0.12	+2.8(5)	2.76
823	0.804	0.558	3.9(5)	0.31	0.55	+3.6(5)	3.62
752	0.809	0.526	0.7(5)	0.09	0.18	+0.6(5)	0.01
009	0.824	1.000	1.5(5)	0.45	0.60	+1.0(5)	0.00
447	0.824	0.802	1.8(3)	0.03	0.07	+1.8(3)	1.69
663	0.824	0.556	3.6(6)	0.04	0.11	+3.6(6)	3.82
841	0.824	0.506	4.2(4)	0.16	0.28	+4.0(4)	4.24

domains with $\vec{\tau} \parallel \vec{a}$ and $\vec{\tau} \parallel \vec{b}$ are equally likely and will give rise to $\langle 110\rangle$-type reflections that, in the laboratory framework, will be indexed as (011) and (101), respectively. When the intensities of these reflections are compared, the domain populations are equal within experimental error. In an attempt to influence the domain population, the single crystal of UO_2 was cooled through T_N in a magnetic field of 60 kOe, $\vec{H} \parallel [1\bar{1}0]$, but no change was observed in the domain population.[16] The magnetic moment direction of the uranium atom is known to lie in the (001) plane (see Fig. 1), but its exact direction in this plane cannot be determined with a multidomain sample.

The elastic magnetic cross section is given by

$$d\sigma_M = \tfrac{1}{3}q^2|M|^2 \quad \text{b/mole}, \tag{5}$$

where the factor of $\frac{1}{3}$ arises from the number of possible magnetic domains, q^2 is the square of the magnetic interaction vector, M is the magnetic structure factor $= 0.2696\mu f(\vec{\kappa})e^{-W_U} \times 10^{-12}$ cm, μ is the magnetic moment per uranium ion in Bohr magnetons and $\vec{\kappa}$ is the scattering vector $[\kappa = 4\pi(\sin\theta/\lambda)]$. The magnetic intensity then becomes

$$I_M = q^2(\tfrac{1}{3}C)[0.2696\mu f(\vec{\kappa})]^2 \times e^{-2W_U}Ay/\sin 2\theta \quad \text{b/mole}, \tag{6}$$

where quantities not defined above appear in Eq. (3). As we shall see in Sec. III, this formula relating $d\sigma_M$ and $f(\vec{\kappa})$ is an oversimplification in UO_2, for which large orbital effects are present. Nevertheless, the concept of an effective magnetic form factor as defined by Eq. (6) is still useful for illustrative purposes.

The intensities of 1250 magnetic Bragg reflections, reducing to 71 independent values of *hkl*, were collected with the crystal at 4.2 K. As with the nuclear reflections, corrections have been made for absorption and extinction, the latter insignificant except for the two most intense reflections. Following Eq. (6), the magnetic intensities were reduced to values of $d\sigma_M$ (Table II) and $\mu f(\vec{\kappa})$. The values of C and $W_U = B_U(\sin^2\theta)/\lambda^2$ were taken from Table I. The square of the magnetic interaction vector q^2 is given by $q^2 = (\frac{1}{2}h^2 + \frac{1}{2}k^2 + l^2)/(h^2 + k^2 + l^2)$. The standard deviations given in Table II are based on both the counting statistics and the internal consistency of a set of equivalent reflections. The values of $\mu f(\vec{\kappa})$ are plotted as a function of $(\sin\theta)/\lambda$ in Fig. 3. A comparison with the limited data presented by Frazer *et al.*[1] shows that, within the quoted uncertainties, the two experiments are in agreement. Following the temperature dependence of the magnetic intensities, we obtain $T_N = 30.7 \pm 0.1$ K, again in excellent agreement with Frazer *et al.*[1] As an additional check, we have examined a second (larger) crystal of UO_2 cut from the same boule. Although serious multiple-scattering effects were observed with this large crystal, an examination of pairs of reflections at the same values of $(\sin\theta)/\lambda$ confirmed the anisotropy shown in Fig. 3.

III. CALCULATION OF MAGNETIC CROSS SECTION

Uranium dioxide is an ionically bonded semiconductor with two $5f$ electrons surrounding each U^{4+} ion. The Russell-Saunders Hund's rule ground

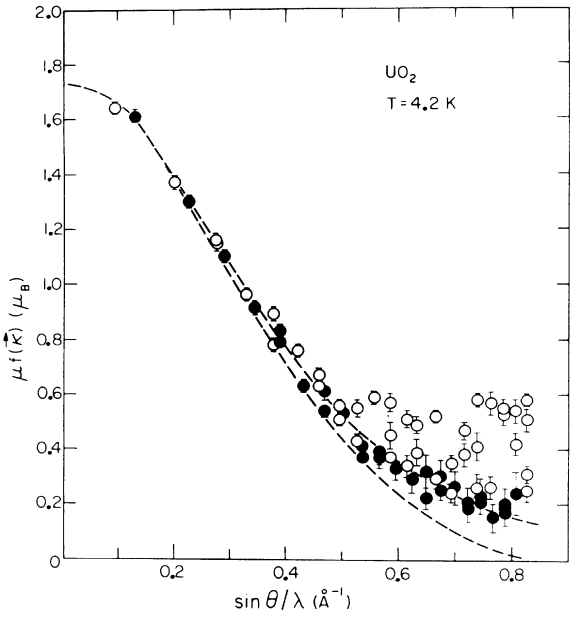

FIG. 3. Experimental values of $\mu f(\vec{\kappa})$ for UO_2 at 4.2 K. The open circles are magnetic reflections with h,k even and l odd; the closed circles are reflections with h,k odd and l even. The broken line encloses an envelope containing the calculated values of $\mu f(\vec{\kappa})$. See Sec. III.

state is $^3H_4$. In the presence of a cubic crystalline field, the ninefold degeneracy of the $^3H_4$ state is reduced to four nondegenerate levels, two triplets Γ_5 and Γ_4, a doublet Γ_3, and a singlet Γ_1. Rahman and Runciman[17] (RR) have performed a complete diagonalization of the Hamiltonian for UO_2 including Coulomb, spin-orbit, and crystal-field terms. They find that the Γ_5 triplet is the ground state. In the notation of Lea, Leask, and Wolf[18] the parameters $x \simeq 0.9$ and $W > 0$. The signs of these values are consistent with the point-charge model. In order of increasing energy, the crystal-field levels are Γ_5, Γ_3, Γ_4, and Γ_1. (An alternative convention used by RR labels the levels T_2, E, T_1, and A_1, respectively.)

When the magnetic cross section is calculated from the induced magnetic moment in the paramagnetic state,[9] we considered both the simple $^3H_4 - \Gamma_5$ triplet and the mixed-J configuration proposed by RR. Since the $^3H_4$ state makes up ~87% of the RR ground state, it is not surprising that the magnetic cross sections from these two states are quite similar. In both cases, the theoretical values of $\mu f(\vec{\kappa})$ scatter closely about a smooth curve that decreases rapidly with $\vec{\kappa}$. We note, however, that the points at large values of $(\sin\theta)/\lambda$ in Fig. 3 exhibit considerable anisotropy. For example, at $(\sin\theta)/\lambda = 0.8$ Å^{-1}, the values of $\mu f(\vec{\kappa})$ vary between 0.2 and 0.6 μ_B. Anisotropy of this magnitude is not predicted by the RR ground-state configuration.[9]

These general remarks concerning Fig. 3 raise the question of whether the magnetization distributions in the ordered and paramagnetic states are fundamentally different. In an attempt to explain the first-order phase transition, Blume[19] proposed that the ground-state wave functions are different in the ordered and paramagnetic states. Alternatively, Allen[20] has proposed a strong spin-lattice interaction as the essential driving force for the first-order transition. Can the strong spin-lattice interaction lead to sufficient polarization of the ground state so that the magnetization density becomes highly aspherical? We should also consider whether, in the ordered state, UO_2 is a simple collinear antiferromagnet. If UO_2 is not type I, then incorrect values of q^2 will have been used in Eq. (6). Since no comparable experiments on actinide antiferromagnets have been reported, we cannot automatically reject any of these possibilities.

To investigate these questions, we have performed a series of cross-section calculations for the U^{4+} ion in UO_2. The magnetic scattering length is defined as a vector $\vec{E}$, with spherical components E_Q given by

$$(2\pi\hbar/m)E_Q = \langle \psi_e | T_Q^K(e,\vec{\kappa}) | \psi_e \rangle . \tag{7}$$

The electron wave functions are represented by ψ_e, and $T_Q^K(e,\vec{\kappa})$ defines a tensor operator. The neutron-electron interaction is expressed as a tensor of rank one, so that we need to evaluate three terms, $Q = 0, \pm 1$. The presence of an unquenched orbital moment means that the magnetization density is a vector quantity[21,22] with three components, M_x, M_y, and M_z. We may associate the components E_Q as follows: $E_0 \rightarrow M_z$, $E_{+1} \rightarrow -(M_x + iM_y)/\sqrt{2}$, and $E_{-1} \rightarrow (M_x - iM_y)/\sqrt{2}$. The magnetic moment density is therefore obtained by Fourier transforming M_x, M_y, and M_z. To compare theory and experiment, we calculate the magnetic cross section

$$\left(\frac{d\sigma}{d\Omega}\right)_M \propto \vec{E}\cdot\vec{E} = E_0^2 - 2E_{-1}E_1 \tag{8}$$

and reduce the theoretical cross sections to $\mu f(\vec{\kappa})$ values by using Eq. (5). We can treat these values as an effective form factor, which is useful when comparing experiment and theory. However, the Fourier inversion of $\mu f(\vec{\kappa})$ does not necessarily give the magnetization density.

Before experiment and theory can be compared in detail, the domain averaging must be considered. As noted previously (see Sec. II B), the populations of the $\vec{a}$, $\vec{b}$, and $\vec{c}$ domains are equal to within ~1%. Therefore, no averaging need be performed

TABLE III. Tabulation for two reflections at $(\sin\theta)/\lambda = 0.788$ Å^{-1} to illustrate domain averaging. The observable quantity is given by the average value in the last column.

State	$\vec{H}$	hkl	q^2	$f(\vec{\kappa})$	$d\sigma_M$ (mb/mole)	$\langle d\sigma_M \rangle$ (mb/mole)
$^3H_4$ free ion	[110]	(734), (374)	0.892	0.0606	0.234	0.122
		$(7\bar{3}4)$, $(\bar{3}74)$	0.324	0.0204	0.010	
	[110]	(750), (570)	0.973	0.0589	0.241	0.121
		$(7\bar{5}0)$, $(\bar{5}70)$	0.027	−0.0364	0.002	
$^3H_4$ Γ_5	[110]	(734), (374)	0.892	0.0601	0.236	0.190
		$(7\bar{3}4)$, $(\bar{3}74)$	0.324	0.0777	0.143	
	[110]	(750), (570)	0.973	0.0441	0.138	0.092
		$(7\bar{5}0)$, $(\bar{5}70)$	0.027	−0.1534	0.046	
$^3H_4$ Γ_5	[100]	(734), $(7\bar{3}4)$	0.338	0.1064	0.280	0.190
		$(\bar{3}74)$, (374)	0.878	0.0393	0.099	
	[100]	(750), $(7\bar{5}0)$	0.338	0.0836	0.173	0.092
		$(\bar{5}70)$, (570)	0.662	0.0158	0.012	
$4J$ Γ_5	[100]	(734), $(7\bar{3}4)$	0.338	0.1590	0.605	0.374
		$(\bar{3}74)$, (374)	0.878	0.0482	0.144	
	[100]	(750), $(7\bar{5}0)$	0.338	0.0836	0.167	0.100
		$(\bar{5}70)$, (570)	0.662	−0.0265	0.033	

over these types of domains; we simply consider one propagation direction, $\vec{\tau} \parallel \vec{c}$, and use a factor of $\frac{1}{3}$ in relating the nuclear and magnetic cross sections. Within one $\vec{c}$ domain, the magnetic moment lies in the (001) plane. It is over *this* plane that the domain averaging is important. For example, if we choose the moment to be parallel to a cell edge, then $+\vec{a}$, $-\vec{a}$, $+\vec{b}$, and $-\vec{b}$ are all possible directions. Rather than consider the magnetic moment $\vec{\mu}$ aligned in four directions in the (001) plane, the domain averaging may be equally well performed by considering $\vec{\mu}$ fixed and summing the scattering from the appropriate permutation of (hkl) planes. The procedure may be illustrated with the help of Table III. The scattering is a function of κ, the scattering vector $[= 4\pi(\sin\theta)/\lambda]$, and the polar angles Θ and Φ, where Θ is the azimuthal angle between $\vec{\kappa}$ and $\vec{\mu}$ and Φ measures the angle between a fixed reference direction and the projection of $\vec{\kappa}$ into the plane perpendicular to $\vec{\mu}$. In the first eight rows of Table III, $\vec{\mu} \parallel [110]$ so that, for example, the (734) and (374) reflections have the same cross section. Similarly, the cross sections for the $(7\bar{3}4)$ and $(\bar{3}74)$ reflections are identical, but quite different (note the form factors vary by a factor of 3) from the first two. The total scattering is therefore the average of these two entries and is given in the last column. For the $^3H_4$-Γ_5 configuration, we have shown calculations with $\vec{\mu} \parallel [110]$ and $\vec{\mu} \parallel [100]$. As expected, the final (measurable) cross sections are identical for these two moment directions, whereas the individual cross sections used in this averaging differ considerably. It is easy to show that this result is quite general and applies for an arbitrary direc-

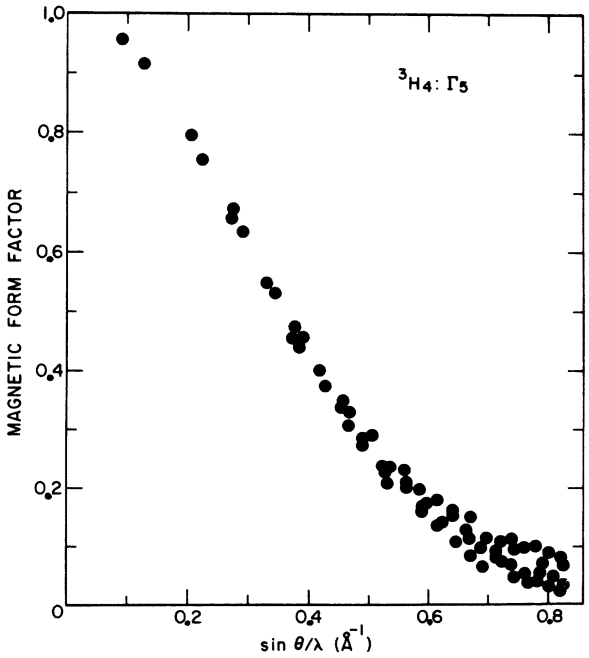

FIG. 4. Effective magnetic form factor of the $^3H_4$-Γ_5 configuration.

tion of the moment in the (001) plane. The problem in UO_2 is not the equivalence of the scattering cross sections for different moment directions but rather that the domain averaging [caused by the moment lying in the (001) plane] prevents us from obtaining direct information about the intrinsic anisotropy in the system.

The values of $f(\vec{\kappa})$ derived from the $^3H_4$-Γ_5 calculation are shown in Fig. 4. A comparison with Fig. 3 suggests that at low angles the cross sections can be brought into agreement with the correct choice of μ, the magnetic moment. A detailed comparison leads to a value for the observed magnetic moment at 4.2 K of $(1.74 \pm 0.02)\mu_B$/U atom, a value somewhat lower than the 1.78 μ_B given by Frazer *et al.*[1] Although the points in Fig. 4 do not lie on a smooth curve as a function of $(\sin\theta)/\lambda$, the anisotropy in the observed form factor is clearly much greater than in the calculation. To demonstrate this, we have drawn the envelope containing the calculated points as broken lines in Fig. 3. The results of calculations including intermediate coupling and J mixing with the RR model for UO_2 are also given in Table II. The differences between the calculations with the RR and $^3H_4$ - Γ_5 models are relatively small because (a) the $^3H_4$ ground state makes up ~87% of the RR ground state (see Table II of Ref. 9), (b) both wave functions have Γ_5 symmetry, (c) the domain averaging reduces the measured anisotropy, and (d) the major differences between the single and mixed-J calculations are in coefficients of the higher-order radial integrals[8] $\langle j_4\rangle$ and $\langle j_6\rangle$. However, the absolute values of these integrals are small. The increase in anisotropy as one progresses from the free ion to the 4J model is illustrated in Table III.

As part of a further investigation into the possible origin of the anisotropy in Fig. 3, we have considered scattering from (i) different ground states of the $^3H_4$ manifold, (ii) the Γ_5 states of excited SLJ manifolds, and (iii) magnetic moments raised out of the (001) plane in the UO_2 magnetic structure.

(i) Scattering from the $^3H_4$-Γ_1 singlet configuration, which would correspond to $W<0(x=1)$ in the Lea, Leask, and Wolf notation, has been discussed in connection with our analysis[8] of the results[23] from US. Since a moment of ~1.7 μ_B arises from a strong polarization of the singlet wave function, it is not surprising that the cross section from this state tends to resemble the free-ion cross section and also exhibits even less anisotropy than found for the Γ_5 wave function in Fig. 4. Allen, in his discussion[20] of the magnetic properties of UO_2, proposed that the Jahn-Teller interaction leads to a ground state with a less than fully polarized spin. The Γ_5 wave function has three components

$$\psi_1 = 0.9354\,|M=3\rangle - 0.3536\,|M=-1\rangle\,,$$
$$\psi_2 = 0.7071\,|M=2\rangle - 0.7071\,|M=-2\rangle\,, \qquad (9)$$

and

$$\psi_3 = 0.9354\,|M=-3\rangle - 0.3536\,|M=1\rangle\,.$$

The dipole moments gJ_z of these three states are 2, 0, and $-2\mu_B$, respectively. In the presence of indirect quadrupole-quadrupole coupling,[20] the states become

$$\psi_1' = |\psi_1\rangle\cos\theta' - |\psi_3\rangle\sin\theta'\,,$$
$$\psi_2' = \psi_2\,, \qquad (10)$$
$$\psi_3' = |\psi_1\rangle\sin\theta' + |\psi_3\rangle\cos\theta'\,,$$

where θ' is an adjustable parameter such that $g\langle\psi_1'|J_z|\psi_1'\rangle = 1.74\ \mu_B$. When calculating the elastic cross section from the wave functions of Eq. (10), we note that quadrupole and higher-order moments of ψ_1 and ψ_3 are identical. This implies that the magnetization densities of ψ_1 and ψ_3 are identical, the only difference is that their dipole moments are reversed. Any combination of ψ_1 and ψ_3, such as ψ_1', will therefore have the same magnetic form factor as ψ_1 alone (Fig. 4).

(ii) In the RR model, the magnetic moment is reduced from the $^3H_4$ - Γ_5 value of 2.0 μ_B by the influence of higher SLJ states. The ground-state wave function is

$$\psi(\Gamma_5) = 0.874\,|^3H_4\rangle - 0.331\,|^1G_4\rangle + 0.138\,|^3F_4\rangle$$
$$- 0.195\,|^3F_3\rangle - 0.214\,|^3F_2\rangle - 0.044\,|^1D_2\rangle$$
$$+ 0.055\,|^3P_2\rangle + 0.097\,|^3H_5\rangle + \cdots\,, \qquad (11)$$

where $\psi(\Gamma_5)$ indicates that the Γ_5 component of each SLJ state is used. The cross section from this state, with the small contributions from additional states neglected, is given in Table II and is similar to that from the $^3H_4$-Γ_5 state. However, the question is whether one of these higher states could be responsible for the anisotropy observed in the experimental data (Fig. 3). To answer this question, we have calculated $d\sigma_M$ for each state separately; one of the more unusual, that from the $^3F_3$-Γ_5 configuration, is shown in Fig. 5. In this configuration, $\vec{S}$ and $\vec{L}$ are not parallel so the magnetization density is most unusual, and this is reflected in the effective form factor calculated with Eq. (8). Figure 5 demonstrates the importance of complete calculations for actinide ions. However, not only are the calculated anisotropies in disagreement with experiment, but the occupation of this state would have to be an order of magnitude greater than the ~4% given by RR for the anisotropies to strongly influence the total neutron cross section. A similar situation exists for the other SLJ manifolds.

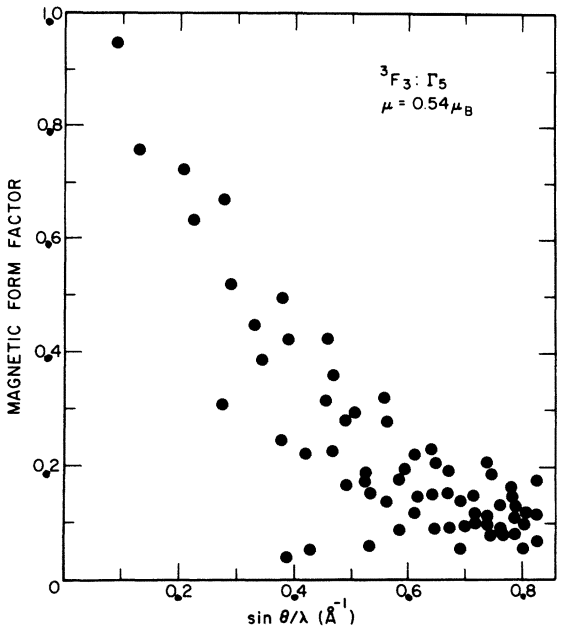

FIG. 5. Effective magnetic form factor of the $^3F_3$-Γ_5 configuration.

(iii) Finally, we have considered raising the magnetic moment out of the (001) plane and calculating the cross section as a function of this angle. As one would expect, the changes in the cross section are functions of q^2 rather than κ. Hence, the (001) and (110) reflections with $q^2 = 1$ and 0.5, respectively, are the most sensitive to variations in the angle between $\vec{\mu}$ and $\vec{\kappa}$. The agreement between theory and experiment at low κ puts an upper limit of ~5° for the deviation of the magnetic moment from the (001) plane, and this approach cannot be used to explain the anisotropy in Fig. 3.

Based on the calculations discussed in this section, we conclude that the large anisotropy observed in $\mu f(\vec{\kappa})$ at large κ is not magnetic in origin. An additional indication of this is the division of reflections in Fig. 3 into those with h,k even and l odd (open circles) and those with h,k odd and l even (closed circles). This division has no relationship to q^2, nor to the spherical coordinates Θ and Φ that relate $\vec{\mu}$ to $\vec{\kappa}$, all of which appear in the expression for the cross section. However, Fig. 3 suggests that almost all the l even points lie within the envelope spanned by the broken lines, whereas, for $(\sin\theta)/\lambda > 0.5$ Å^{-1}, the l odd points lie substantially above the upper limit of the calculations. We can represent the behavior of the two subsets more clearly by plotting the difference cross section $(d\sigma_{obs} - d\sigma_M)$ in Fig. 6. This shows immediately that the l even points are in excellent agreement with theory. The small residual scattering of ~0.3 mb/mole observed for

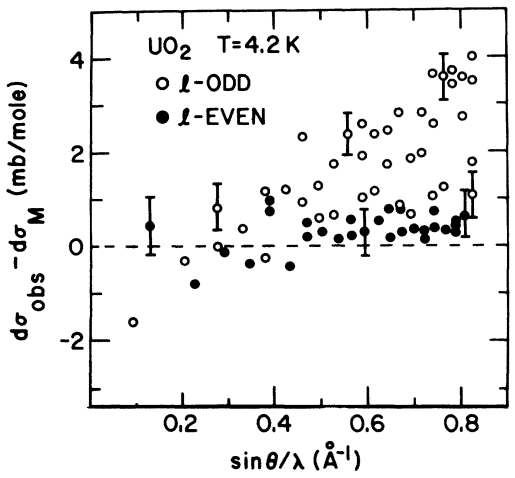

FIG. 6. Difference cross section $d\sigma_{obs}$ (observed)-$d\sigma_M$ (calculated) plotted for each Bragg reflection. The open circles are reflections with h,k even and l odd; the closed circles are reflections with h,k odd and l even.

the l even points is probably a consequence of multiple scattering (see Sec. II). The most important point of Fig. 6 is that the l odd reflections exhibit additional intensity which cannot be understood on the basis of magnetic scattering from isolated ions.

IV. DEFORMATIONS OF THE OXYGEN SUBLATTICE

In the previous section, we have shown that the anisotropy in the neutron cross section at high κ cannot arise from magnetic scattering associated with the U^{4+} ions. The measurements in the paramagnetic state[9] are in good agreement with theory and show much less anisotropy at high κ than in Fig. 3. The presentation of the difference cross section $(d\sigma_{obs} - d\sigma_M)$ in Fig. 6 suggests that additional scattering is present only at the l odd magnetic reciprocal lattice points. The nuclear structure factors of the ideal fluorite atomic arrangement are zero for the magnetic reciprocal lattice points, but we must now consider whether small displacements of the atoms can give rise to the nonzero cross section of Fig. 6.

One way to check for the presence of simultaneous nuclear and magnetic scattering is to examine the particular Bragg reflection with a beam of polarized neutrons. Under ideal conditions, the nuclear-magnetic interference term, and therefore the intensity of the reflection, will be polarization sensitive. This experiment was attempted on a number of reflections from UO_2, but the intensities were independent of the neutron polarization. On the other hand, both the equidomain nature of the sample and the possibility that the

magnetic and nuclear intensities arise from different domains lead to the intensities independent of neutron polarization. A more direct way to determine whether the intensities arise from nuclear or magnetic interactions is to analyze the polarization of the scattered neutrons,[24] but the weakness of the intensities of interest make this impractical at the CP-5 facility.

A. Lattice modes (q=0)

To investigate if the additional scattering in Fig. 6 can arise from atomic displacements, we consider the local modes of the oxygen cube surrounding a U^{4+} ion. This problem has been treated in two elegant papers by Allen.[20] Let us first determine the lattice modes of a nine-atom assembly consisting of a metal atom at the center of a cube and eight oxygen atoms at the cube corners. The lattice modes (with their degeneracies) are $T_{1u}(3)$—the translation of the center of mass; $T_{1g}(3)$—the rigid rotation of the cube; and the vibrational modes $A_{1g}(1)$, $E_g(2)$, $2T_{2g}(6)$, $A_{2u}(1)$, $E_u(2)$, $2T_{1u}(6)$, and $T_{2u}(3)$.

The ground state of the U^{4+} ion is the Γ_5 triplet (T_2 symmetry), so coupling between two uranium ions takes place via lattice modes that are contained in the symmetric square $[\Gamma_5^2]$

$$\Gamma_5 \times \Gamma_5 = A_{1g} + T_{1g} + E_g + T_{2g}. \tag{12}$$

The modes satisfying this condition are one A_{1g} mode, one T_{1g}, one E_g, and two T_{2g} modes. The A_{1g} (breathing) and T_{1g} (rotation) modes preserve the cubic point group symmetry of each atom so the vibrational modes of interest are E_g and T_{2g}. These two modes are shown in Fig. 7. The two

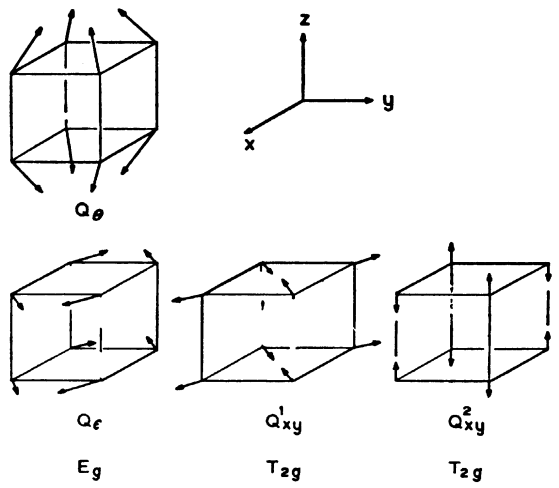

FIG. 7. Homogeneous deformations with E_g and T_{2g} symmetry that mix Γ_5 states. One component of each mode is shown. (After Allen, Ref. 20.)

components of the E_g mode, Q_ϵ and Q_θ, correspond to orthorhombic and tetragonal deformations, respectively. In Allen's notation, the T_{2g} modes are Q^1 and Q^2. The Q^1 mode corresponds to a shear deformation and leads to a monoclinic unit cell. The Q^2 mode, in which the two oxygen tetrahedra move out of phase, corresponds to an optic phonon. It is important to stress that all these deformations are homogeneous. In the long wavelength limit, these represent $q = 0$ phonons and each deformation, except the Q^2 mode, can be identified with a corresponding reduction in the symmetry of the overall unit cell. We characterize these static effects as *external* distortions. In the case of the $T_{2g}(Q^2)$ mode, which corresponds to a $q = 0$ optic phonon, the dimensions of the overall unit cell remain the same as in the cubic phase. The Q^2 mode is characterized as an *internal* distortion.

B. External distortions

Cracknell and Daniel[25] have stressed that the symmetry of UO_2 in the ordered state can be no higher than orthorhombic, so we should certainly anticipate some departure from the equal dimensions ($a = b = c$, $\alpha = \beta = \gamma = 90°$), which characterize the paramagnetic state. The para- to antiferromagnetic transition in UO_2 is first order.[1] This implies a discontinuity in the volume of the unit cell, and such a discontinuity $\Delta V/V \sim 5 \times 10^{-5}$ was detected by Brandt and Walker[26] by means of strain-gauge techniques. However, because of the multidomain nature of the sample below T_N, this sensitive technique cannot provide information on the unit-cell dimensions in the ordered phase. A number of x-ray experiments have been performed on UO_2 at low temperature, but we have not found any published reports. The first reference to an x-ray experiment designed to determine the unit-cell dimensions at low temperature appears as a private communication in Brandt and Walker[26] (see Ref. 12 of that paper). No departure from cubic symmetry was found. White and Sheard[27] refer more specifically to "precision x-ray measurements of lattice parameters at Harwell... give no broadening of the (600) reflection, which would indicate a tetragonal distortion exceeding a few parts in a million." In a series of experiments on polycrystalline samples of actinide compounds,[28] we have characterized the absence of an external distortion in UO_2 by the quantity $|1 - c/a| \leq 3 \times 10^{-4}$. (This quantity, although referring specifically to a tetragonal distortion, will not change appreciably if distortions of other symmetries are considered.) In principle, our neutron experiments provide information on the lattice symmetry below T_N; but because of intensity requirements, the experi-

mental resolution was rather poor and quantitative information could not be obtained. Recent x-ray experiments[29] at this Laboratory on single crystals have confirmed the previous results that the external distortion in UO_2 is either absent or extremely small.

C. Internal distortions

We have now excluded all the acoustic phonon-like $q=0$ modes that couple to the Γ_5 ground state and turn to the Q^2 optic phonon. This mode was proposed by Allen[20] as the most likely candidate for the virtual-phonon coupling in UO_2. Let us consider whether this mode can contribute to the additional reflections shown in Fig. 6. We choose four of the oxygen atoms, sublattice A, described by the vectors (see Fig. 1 or Fig. 7)

$$\vec{t}_1=(\tfrac{1}{4},\tfrac{1}{4},\tfrac{1}{4});\quad \vec{t}_2=(\tfrac{3}{4},\tfrac{3}{4},\tfrac{1}{4});$$
$$\vec{t}_3=(\tfrac{3}{4},\tfrac{1}{4},\tfrac{3}{4});\quad \vec{t}_4=(\tfrac{1}{4},\tfrac{3}{4},\tfrac{3}{4}). \tag{13}$$

In the Q^2 motion, all oxygen atoms of one sublattice are displaced a constant amount $\vec{r}$ leading to a nuclear structure factor from these four atoms of

$$N_A=\sum_{i=1}^{4}\exp[i\vec{\kappa}\cdot(\vec{t}_i+\vec{r})]$$
$$=\exp(i\vec{\kappa}\cdot\vec{r})\left[\sum_{i=1}^{4}\exp(i\vec{\kappa}\cdot\vec{t}_i)\right]. \tag{14}$$

The term in brackets here is simply the face-centering condition, i.e., it is zero unless h, k, and l are all even or all odd. Therefore, $N_A=0$ for the reflections shown in Fig. 6, since all have mixed indices. Similarly, the oxygens on sublattice B do not contribute to N_A. The Q^2 modes will modify the intensities of the fundamental Bragg reflections, but such changes in intensity will be difficult to detect. Hence, a small internal distortion with Q^2 symmetry could not be observed by the present neutron experiments. Pirie and Smith[30] found no evidence for an internal distortion of the uranium sublattice. Our results are also in agreement with this statement.

The absence of any appreciable external distortion and the failure of the Q^2 internal mode to account for the additional intensities shown in Fig. 6 lead us to consider *inhomogeneous* deformations. By this, we mean deformations that are not identical as one moves from uranium to uranium in the lattice. One way to obtain inhomogeneous deformations is to form linear combinations of the modes in Eq. (12). Two simple inhomogeneous deformations, which correspond to zone boundary $q=(2\pi/a)(1,0,0)$ phonons, are shown in Fig. 8. In Fig. 8(a), a $T_{2g}(Q^1)$ shear deformation is combined with the T_{1g} pure rotation, but with the sense

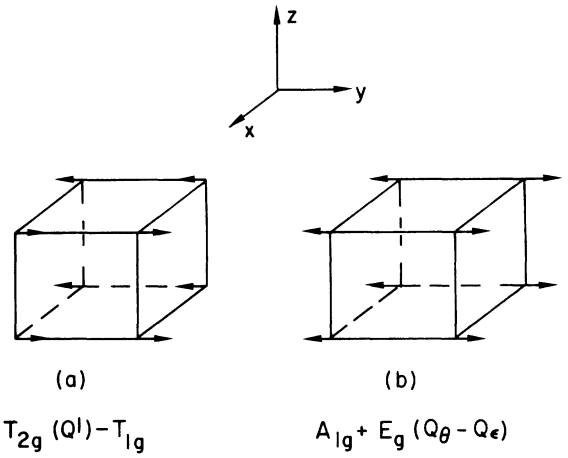

FIG. 8. Inhomogeneous deformations (linear combinations of the normal modes) of the cube of oxygen atoms surrounding each metal atom that mix Γ_5 states. One component of each mode is shown.

of the atomic displacement of the nearest-neighbor oxygen atoms rotated by π between adjacent uranium atoms. This corresponds to a transverse phonon. In Fig. 8(b), an E_g deformation is combined with an A_{1g} uniform dilation. This corresponds to a longitudinal phonon. Since these modes are degenerate, the combinations can be made in a variety of ways. Thus, the (Q^1-T_{1g}) mode is sixfold degenerate, and the $(A_{1g}+E_g)$ mode is threefold degenerate. In all these deformations, the uranium sublattice remains undisturbed.

To test whether these deformations can explain the additional intensity of Fig. 6, we first note that neither mode contributes to the l even magnetic reciprocal lattice points. The solid points (l even) in Fig. 6 are thus only magnetic, as we had expected from their near zero residuals. To examine the l odd reflections, we have performed a least-squares refinement with the quantities $(d\sigma_{\text{obs}}-d\sigma_M)$ of Fig. 6 as experimental input. The calculated cross section $d\sigma_D$ arises from displacements of the oxygen atoms from their ideal fluorite positions. The only parameters in the refinements are Δ_T and Δ_L, where these are fractional coordinate shifts of the oxygen atoms perpendicular to (transverse) or parallel to (longitudinal) the propagation direction of the phonon. As with the magnetic calculations, we must perform the domain averaging when comparing intensities from a multidomain crystal, and this leads to an inability to distinguish $\Delta_T(x)$ and $\Delta_T(y)$, assuming the mode propagates along z. The results for least-squares fit with Δ_T and Δ_L are displayed separately in Figs. 9(a) and 9(b), which correspond to the motions shown in Figs. 8(a) and 8(b), respectively. In Fig. 9(a), the fit is clearly excellent ($\chi^2=1$), whereas

the (E_g+A_{1g}) longitudinal mode, Fig. 9(b), cannot account for the neutron intensities ($\chi^2=21$). We have allowed Δ_T and Δ_L to vary simultaneously in the least-squares fit, but such refinements lead to a negligible value for Δ_L and no significant improvement in the fit. Therefore, the longitudinal (E_g+A_{1g}) mode plays no significant role in the spin-lattice interaction. The least-squares fit of $d\sigma_D$ and $(d\sigma_{obs}-d\sigma_M)$ shown in Fig. 9(a) gives $\Delta_T = \Delta = (2.6\pm0.2)\times10^{-3}$, which implies a shift of 0.014 Å in the oxygen position. The points remaining outside 2σ in Fig. 9(a) are those of the type $(00l)$. We assume these reflections, which lie on a line of high symmetry in the reciprocal lattice, may suffer from multiple scattering effects. The values of $d\sigma_D$ are given in Table II.

V. SUMMARY

A. Magnetic cross section

In Sec. III, we have presented details of calculations of the magnetic cross section from the U^{4+} ions in antiferromagnetically ordered UO_2. The higher SLJ states in the RR ground-state wave function do not significantly modify the cross section from the $^3H_4$ state. Therefore, previous calculations confined to the Russell-Saunders Hund's rule configurations for uranium ions[8,23] may not be significantly modified by the introduction of intermediate coupling and J mixing. This statement will *not* be true for plutonium ions, in which case the Russell-Saunders ground state is known to be appreciably modified.[6] Moreover, in the light of our rather complete understanding of the scattering cross section from UO_2, we have attempted to test which of the cross-section calculations ($^3H_4$ or $4J$) of Table II best fits the data. Therefore, we have restricted the comparison to the reflections with l even, for which $d\sigma_D=0$. We define the quantity

$$\chi^2=\sum\left(\frac{d\sigma_{obs}-d\sigma_M}{\Delta d\sigma_{obs}}\right)^2\Big/ n\,, \tag{15}$$

where the sum is over the l even reflections, and $\Delta d\sigma_{obs}$ is the experimental error on $d\sigma_{obs}$. The results are $\chi^2(^3H_4)=1.28$ and $\chi^2(4J)=1.73$. Thus, although both calculations fit the experimental data well, the $^3H_4$ cross section appears to be the best fit. No direct observation of the crystal field energy levels has been reported in metallic actinide materials; the parameters used by RR were based on optical studies of ionic compounds. Recent neutron experiments[31] on the NaCl compound USb have also shown that the simple Russell-Saunders ground state gives an excellent description of the neutron cross section.

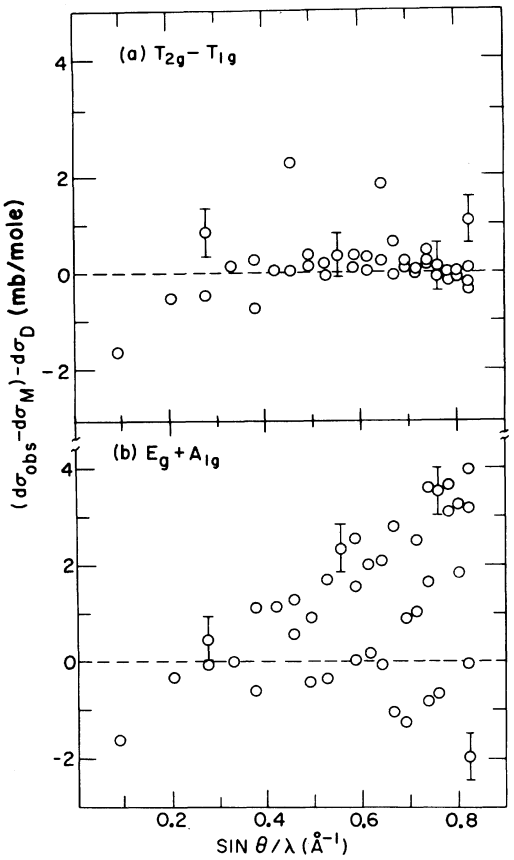

FIG. 9. Residual cross sections plotted for reflections with l odd after subtracting $d\sigma_D$ (arising from the inhomogeneous deformation of the oxygen sublattice) from the $(d\sigma_{obs}-d\sigma_M)$ values of Fig. 6. The calculations of $d\sigma_D$ in (*a*) and (*b*) use the modes of Fig. 8(a) and 8(b), respectively.

B. Magnetoelastic interactions

In Sec. IV, we have shown that the additional scattering shown in Fig. 6 is caused by an oxygen displacement of 0.014 Å from the ideal fluorite positions. It is worth pointing out that at low temperatures the oxygen temperature factor (Table I) is $B_0=0.22$ Å^2 so that the mean thermal amplitude $\langle u_0\rangle=(B/8\pi^2)^{1/2}=0.053$ Å. Therefore, the static displacements are quite small in terms of the lattice vibrations. Instead of the $T_{2g}(Q^2)$ internal mode providing the mechanism for U-U coupling, as proposed by Allen,[20] the modes that dominate the cooperative Jahn-Teller effect are the oxygen internal shear deformations $T_{2g}(Q^1)-T_{1g}$. This linear combination of Q^1 and T_{1g} rotation, rather than pure Q^1, does not affect the coupling between Γ_5 states. Therefore, the dominance of the internal shear deformation is compatible with the essential features of Allen's theory that explain the first-order magnetic transition with no external

distortion.

The coupling with the T_{2g} shear deformations is also compatible with the anomalous softening of the C_{44} elastic constant[26] at temperatures extending far above T_N. Similar variations in the elastic constants of rare-earth compounds above their ordering temperatures have been attributed to magnetic quadrupole-quadrupole interactions.[32] In UO_2, the presence of strong spin-lattice interactions was firmly established by the experiments of Cowley and Dolling,[33] who observed an anticrossing in the magnon-phonon dispersion relation at 9 K. Our elastic neutron experiment identifies the mode of the internal distortion. An *inelastic* neutron experiment to search for evidence of the dynamic effects of this Jahn-Teller coupling above the ordering temperature would seem eminently worthwhile.

C. Magnetic structure

If the propagation direction of the magnetic structure is parallel to the $\vec{c}$ axis, then in Fig. 8(a) the phonon and magnetic propagation directions are perpendicular $\vec{\tau}_D \perp \vec{\tau}_M$. We illustrate this more clearly in Fig. 10. Here $\vec{\tau}_D \parallel \vec{a}$ (note that we restrict our consideration to transverse phonons in light of Sec. IV), whereas $\vec{\tau}_M \parallel \vec{c}$. An alternative model in which $\vec{\tau}_D \parallel \vec{\tau}_M$ is equally possible. To visualize this in Fig. 8(a), imagine that the top and bottom, rather than front and back, faces are sheared. On the basis of the neutron intensities, we cannot distinguish between these two models. However, the driving force for the interactions in UO_2 is the quadrupole moments of the U^{4+} ion. The magnetization density of the function ψ_1 in Eq. (7) is oblate (i.e., it resembles a compressed sphere with the quantization axis or dipole moment parallel to the compression axis) so that the electrostatic interaction would seem to favor the spin configuration shown in Fig. 10. The spins here are aligned parallel to the shortest diagonal of the parallelopiped formed by the oxygen atoms. The resultant magnetic structure is a four sublattice model, rather than the simple two sublattice model assumed heretofore for UO_2. A calculation of the magnetic structure factors for the two (Fig. 1) and four (Fig. 10) sublattice models gives $\mu f(\vec{\kappa})$ and $\mu f(\vec{\kappa})/\sqrt{2}$ per uranium atom, respectively. However, the domain factors for the same two magnetic configurations are $\frac{1}{3}$ and $\frac{2}{3}$, respectively. Substitution into Eq. (4) thus leaves $d\sigma_M$ unchanged. The four sublattice model may also explain some of the unusual features of the infrared and Raman spectra[34] and would seem a natural consequence of the oxygen deformation, as illustrated in Fig. 10.

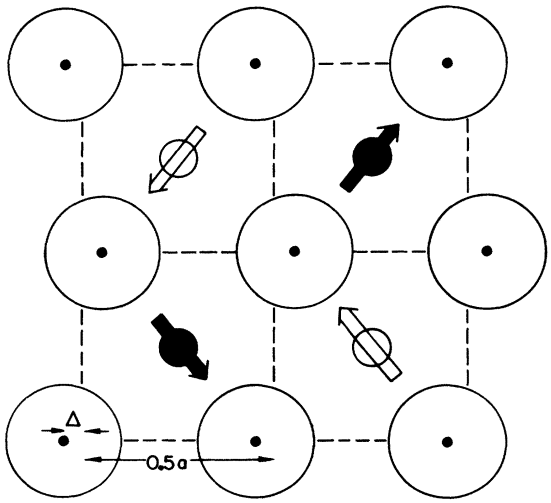

FIG. 10. (001) projection of the fluorite structure. The closed and open circles represent uranium atoms at $z=0$ and $z=\frac{1}{2}$, respectively. The large circles represent oxygen atoms at $z=\frac{1}{4}$ and $z=\frac{3}{4}$ displaced from the ideal fluorite lattice (indicated by the dashed lines). The shift of the oxygen atoms is not drawn to scale, $\Delta/a = 2.6\times10^{-3}$. The suggested noncollinear spin configuration is also shown.

Our conclusions suggest the need for several additional experiments. Section V A discusses the need for direct information on the Γ_5-Γ_3 crystal field splitting, which RR have predicted as 180 meV. We plan to measure this transition using a high-energy transfer spectometer at the Argonne pulsed neutron source. We are presently measuring the temperature dependence of the oxygen sublattice internal rearrangement to obtain information about the strength of the magnetoelastic interaction in UO_2. The need to remeasure the magnon-phonon interaction has already been discussed in Sec. V B. The internal rearrangement observed in UO_2 may also occur in NpO_2, in which a number of experiments have observed an anomaly at 25 K. Mössbauer experiments[35] show that the 25 K transition is nonmagnetic, and the small line broadening at low temperatures could arise from an electric quadruple moment at the Np site caused by a shift in the oxygen atoms. A neutron experiment to investigate this possibility is planned.

ACKNOWLEDGMENTS

We would like to express our thanks to M. H. Mueller and R. L. Hitterman for experimental assistance, to A. J. Freeman, D. J. Lam, and S. K. Chan for advice on the magnetic cross-section calculations, and to B. R. Cooper for his participation in developing the ideas on the internal distortion. It is a pleasure to thank S. J. Allen for pointing out the relevance of the four-sublattice spin structure.

*Work supported by the U. S. Energy Research and Development Administration.

[1]B. C. Frazer, G. Shirane, D. E. Cox, and C. E. Olsen, Phys. Rev. 140, A1448 (1965).
[2]B. T. M. Willis and R. I. Taylor, Phys. Lett. 17, 188 (1965).
[3]D. F. Johnston, Proc. Phys. Soc. Lond. 88, 37 (1966); S. W. Lovesey and D. E. Rimmer, Rep. Prog. Phys. Lond. 32, 333 (1969); W. Marshall and S. W. Lovesey, *Theory of Thermal Neutron Scattering* (Oxford U.P., London, 1971).
[4]E. Balcar, S. W. Lovesey, F. A. Wedgwood, J. Phys. C 3, 1292 (1970); G. H. Lander and T. O. Brun, J. Chem. Phys. 53, 1387 (1970).
[5]T. O. Brun and G. H. Lander, Phys. Rev. Lett. 29, 1172 (1972); G. H. Lander, T. O. Brun, and O. Vogt, Phys. Rev. B 7, 1988 (1973).
[6]*The Actinides: Electronic Structure and Related Properties*, edited by A. J. Freeman and J. B. Darby (Academic, New York, 1974), Vol. I, Chap. 1.
[7]J. Faber, Jr., AIP Conf. Proc. 24, 51 (1975).
[8]A. J. Freeman, J. P. Desclaux, G. H. Lander, and J. Faber, Jr., Phys. Rev. B 13, 1168 (1976).
[9]G. H. Lander, J. Faber, Jr., A. J. Freeman, and J. P. Desclaux, Phys. Rev. B 13, 1177 (1976).
[10]J. Faber, G. H. Lander, and B. R. Cooper, Phys. Rev. Lett. 35, 1770 (1975); AIP Conf. Proc. 29, 379 (1976).
[11]R. K. Edwards, S. M. Chandrasekhardish, and P. M. Davidson, High Temp. Sci. 1, 98 (1969).
[12]L. Lynds, J. Inorg. Nucl. Chem. 24, 1007 (1962).
[13]L. Heaton, M. H. Mueller, M. F. Adam, and R. L. Hitterman, J. Appl. Cryst. 3, 289 (1970).
[14]W. H. Zachariasen, Acta Crystallogr. 23, 558 (1967).
[15]K. D. Rouse, B. T. M. Willis, and A. W. Pryor, Acta Crystallogr. B 24, 117 (1968).
[16]This experiment argues strongly against the presence of a small ferromagnetic component, as proposed by P. D. Hambourger and J. A. Marcus, Phys. Rev. 157, 438 (1967). Such a ferromagnetic component would align with the external magnetic field and lead to a modification of the domain population.
[17]H. U. Rahman and W. A. Runciman, J. Phys. Chem. Solids 27, 1833 (1966); 30, 2497 (1969); H. U. Rahman, Physica (Utr.) 45, 511 (1970).
[18]K. R. Lea, M. J. M. Leask, and W. P. Wolf, J. Phys. Chem. Solids 23, 1381 (1962).
[19]M. Blume, Phys. Rev. 141, 517 (1966).
[20]S. J. Allen, Phys. Rev. 166, 530 (1968); 167, 492 (1968).
[21]O. Steinsvoll, G. Shirane, R. Nathans, M. Blume, H. A. Alperin, and S. J. Pickart, Phys. Rev. 161, 499 (1967).
[22]E. Balcar, J. Phys. C 8, 1581 (1975).
[23]F. A. Wedgwood, J. Phys. C 5, 2427 (1972).
[24]R. M. Moon, T. Riste, and W. C. Koehler, Phys. Rev. 181, 920 (1969).
[25]A. P. Cracknell and M. R. Daniel, Proc. Phys. Soc. Lond. 92, 705 (1967).
[26]O. G. Brandt and C. T. Walker, Phys. Rev. 170, 528 (1968).
[27]G. K. White and F. W. Sheard, J. of Low Temp. Phys. 14, 445 (1974). See Ref. 31 of this paper.
[28]G. H. Lander and M. H. Mueller, Phys. Rev. B 10, 1994 (1974).
[29]J. Faber, Jr. and M. H. Mueller (unpublished).
[30]J. D. Pirie and T. Smith, Phys. Status Solidi 41, 221 (1970).
[31]G. H. Lander, AIP Conf. Proc. 29, 311 (1976).
[32]G. A. Gehring and K. A. Gehring, Rep. Prog. Phys. Lond. 38, 1 (1975).
[33]R. A. Cowley and G. Dolling, Phys. Rev. 167, 464 (1968).
[34]S. J. Allen and P. J. Colwell (private communication, 1975); P. J. Colwell, L. A. Rahn, and C. T. Walker, The Third International Conference on Light Scattering in Solids, Campinas, SP, Brazil, 1975 (unpublished).
[35]B. D. Dunlap, G. M. Kalvius, D. J. Lam, and M. B. Brodsky, J. Phys. Chem. Solids 29, 1365 (1968).